

Journal of Materials Chemistry C

Accepted Manuscript



This article can be cited before page numbers have been issued, to do this please use: X. Li, H. Luo, Y. Wang, X. Wang, J. Cao, L. Wang and M. Peng, *J. Mater. Chem. C*, 2019, DOI: 10.1039/C8TC06453A.



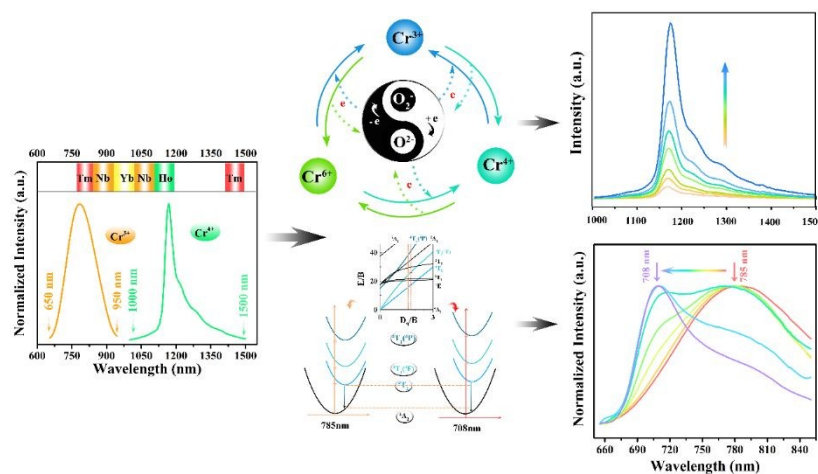
This is an Accepted Manuscript, which has been through the Royal Society of Chemistry peer review process and has been accepted for publication.

Accepted Manuscripts are published online shortly after acceptance, before technical editing, formatting and proof reading. Using this free service, authors can make their results available to the community, in citable form, before we publish the edited article. We will replace this Accepted Manuscript with the edited and formatted Advance Article as soon as it is available.

You can find more information about Accepted Manuscripts in the [author guidelines](#).

Please note that technical editing may introduce minor changes to the text and/or graphics, which may alter content. The journal's standard [Terms & Conditions](#) and the ethical guidelines, outlined in our [author and reviewer resource centre](#), still apply. In no event shall the Royal Society of Chemistry be held responsible for any errors or omissions in this Accepted Manuscript or any consequences arising from the use of any information it contains.

Table of Content only:



Selective self-redox and crystal field modulation have been demonstrated for enhanced and tuned broadband emission in chromium doped versatile glass. More emission ions and more efficient centers were created to enhance the emission intensity by one order. In addition, proper crystal field was equipped to liberate new emission band at ~ 708 nm and enrich emission region.



Selective self-redox and crystal field modulation for enhanced and tuned broadband emission in chromium-doped aluminate glasses

Xingyu Li, Haoyang Luo, Yafei Wang, Xiu Wang, Jiangkun Cao, Liping Wang and Mingying Peng*

Received 00th January 20xx,
Accepted 00th January 20xx

DOI: 10.1039/x0xx00000x

www.rsc.org/

The emerging era of big data has stimulated the development of optical materials with broad emission region to alleviate data transmission of higher capacity and speed. Here, broadband emission, almost covering the region of 650-1500 nm, was realized through doping transition metal ions into versatile aluminate glasses, where abundant micro-structures and certain oxidizing capacity could be guaranteed to enrich emissions. And we targeted to improve spectroscopic properties via simultaneous self-redox and crystal field modulation of Cr ions and matrixes, respectively. More emission ions and more efficient centers were created to enhance the emission intensity by more than one order. In addition, proper crystal field was created to liberate new emission band at ~708 nm. The results may allow developing tunable fiber laser and amplifier with the materials potentially and pave the way to precisely control over valence and crystal field to obtain efficient emission.

1. Introduction

Recently, the emerging era of big data proposes urgent requirements for broadband emission materials to extend new data transmission window to resolve data traffic eventually¹⁻⁴. Also, these optical materials with broad emission region have been pursued in considerable fields of bioimaging and tunable fiber lasers⁵⁻⁸. Yet, the mainly devoted rare-earth (RE) ions activated materials lack sufficient ability to cover all important spectral regions, for instance ~1200-1500 nm. Their limited and fixed emission from intrinsic *f-f* forbidden transition drives it beyond the capacity to meet the needs only by virtue of RE ions⁹⁻¹⁵.

Transition metal ions have been regarded as talented dopants for generating controllable broadband emissions in view of their distinct electronic configuration and tunability with crystal field. In particular, chromium ions with various valence states (from 0 to +6) possess the talent of abundant emission region for the potential electron transitions¹⁶⁻¹⁹. For example, tetrahedrally coordinated tetravalent chromium could bring about 1.1-1.6 μm emission; 1.18-1.32 and 1.36-1.56 μm emission from Cr⁴⁺ doped forsterite and YAG, respectively^{14, 20-23}. And trivalent chromium of octahedral coordination within some matrixes can give birth to emission in ~0.65-1.3 μm region²⁴. Consequently, chromium ions could theoretically endow optical materials with fully rich emission region if abundant proper valences and microstructures were guaranteed in

matrixes. Unfortunately, Cr activated materials, especially for Cr⁴⁺ doped glasses, usually suffer from limited Cr solubility, which restricts their practical applications²⁵⁻²⁸. Improving emission with high efficiency under limited Cr content is of great challenge to confront. One promising key is to transform as many Cr ions as possible in matrixes into luminescent ions or more efficient emission centers, which could be realized by altering Cr valence and creating more proper crystal field, since Cr ions have been demonstrated as valence-transformable and crystal field-dependent emitters¹⁶. Therefore, matrixes are in need to be explored, which could possess the capacity to not only guarantee adequate valence state and surroundings to enrich emission region but also prompt Cr dopant to be efficient emitting ions.

Starting from the view of above points, aluminate glasses were selected as ideal matrixes regarding that the glasses, with no traditional glass network formers, are characterized by the relatively disorder structure, indicating enough sites to create efficient emission centers²⁹⁻³¹. Beyond this, there exist some superoxide ion radicals, which make it possible to adjust Cr ions to desired valence state via self-redox within glasses^{32, 33}.

Inspired by these, we successfully realized broad emission occupying within the region of 650-1500 nm through anchoring transition metal ions in versatile aluminate glasses. And selective self-redox of Cr ions and providing more proper environment took effects in improving the optical performance. That is, the emission intensity is enhanced by a factor of more than 15 and the lifetime is prolonged by 1.5 times successfully. Other than these, a new band at ~708 nm was generated, widening the spectral region, due to crystal field evolution.

2. Experimental section

2.1 Sample preparation

The China-Germany Research Center for Photonic Materials and Devices; The State Key Laboratory of Luminescent Materials and Devices, Guangdong Provincial Key Laboratory of Fiber Laser Materials and Applied Techniques, School of Materials Science and Technology, South China University of Technology, Guangzhou 510640, P. R. China.
E-mail: pengmingying@scut.edu.cn.

Electronic Supplementary Information (ESI) available: [details of any supplementary information available should be included here]. See DOI: 10.1039/x0xx00000x

Cr-doped aluminate glasses, with the nominal molar compositions of $63\text{CaO}-37\text{Al}_2\text{O}_3-x\text{Cr}_2\text{O}_3$ ($x=0, 0.05\%, 0.15\%, 0.25\%, 0.40\%, 0.60\%, 0.80\%$) and $(63-y)\text{CaO}-37\text{Al}_2\text{O}_3-0.25\%\text{Cr}_2\text{O}_3-y\text{SrO}$ ($y=0, 4, 10, 16, 22, 28, 36$) were obtained in air by conventional melting and consequent quenching method, which are denoted as CAzC ($z=1000x, x=0, 0.05\%, 0.15\%, 0.25\%, 0.40\%, 0.60\%, 0.80\%$) and yS ($y=0, 4, 10, 16, 22, 28, 36$) respectively. For instance, $63\text{CaO}-37\text{Al}_2\text{O}_3-0.25\%\text{Cr}_2\text{O}_3$ could be expressed in CA2.5C; and $(63-16)\text{CaO}-37\text{Al}_2\text{O}_3-0.0025\text{Cr}_2\text{O}_3-16\text{SrO}$ is represented by 16S. Raw materials, CaCO_3 , SrCO_3 and Al_2O_3 , were selected in the analytical reagent level; and 99.99% pure Cr_2O_3 was used as the dopant. Each 50 g batch was mixed homogeneously and put in corundum crucibles. Whereafter, the mixtures were melted at $1550\text{ }^\circ\text{C}$ for 0.5 h in an air atmosphere. The melt was poured onto a stainless steel plate and pressed with another stainless plate, by which the glasses samples were prepared successfully. Subsequently, these glasses samples were polished and ground for optical and structural measurements.

2.2 Characterization

Optical properties: The Edinburgh FS920 fluorescence spectrometer equipped with a 450 W Xe lamp and a μF900 microsecond lamp as excitation sources was utilized to obtain static and dynamic-state photoluminescence (PL) and photoluminescence excitation (PLE) spectra along with emission decay spectra. The absorption spectra were collected with Perkin Elmer Lambda 900 Ultraviolet-Visible-Near-infrared (UV-Vis-NIR) spectrophotometer.

Structural properties: X-ray diffraction (XRD) patterns were measured for finely ground samples to verify their amorphous characters using an X-ray diffractometer D/max-III A with $\text{Cu K}\alpha$ radiation ($\lambda = 1.5418\text{ \AA}$). ^{27}Al MAS NMR spectra were performed using a Bruker AVANCE III HD 400 instruments. To analyze the structure evolution, ^{27}Al MAS NMR spectra were recorded at 9.4 T at a frequency of 104.26 MHz using a 3.0l s pulse with a 4 mm MAS probe. Raman spectra were performed on a Raman spectrometer (Renishaw in Via) with a 532 nm wavelength laser as excitation source. The electron paramagnetic resonance (EPR) spectra were recorded under ambient temperature using a Bruker A300 EPR spectrometer operating in the X-band frequency (9.8 GHz). And differential scanning calorimeter (NETZSCH STA 449C) was utilized to measure glass transitions (T_g) and crystallization (T_c) temperatures with the heating rate of $10\text{ }^\circ\text{C}/\text{min}$ to analyze the glass forming ability. All the data were collected at room temperature unless otherwise prescribed.

3. Results and discussion

3.1 Observation of broadband emission of Cr-activated aluminate glasses in 650-1500 nm

Chromium of abundant valence state embodies the natural gift of various electron transitions, which would theoretically liberate outstanding optical emission region if appropriate sites guaranteed. Aluminate glasses were featured by the disordered structure and adequate sites options for lack of traditional glass network formers. Also, a considerable amount of O_2 species

dissolved gifts aluminate glasses with the certain oxidizing capacity to modulate valence state of Cr ions. These enable Cr doped aluminate glasses to exhibit broadband emission region, and photoemission spectra (sample CA2.5C) are depicted in Figure 1 and compared with optical data of RE ions activated materials. When excited at 310 and 670 nm, the emission band lies at ~ 785 and 1175 nm, which originates from Cr^{3+} and Cr^{4+} ions, respectively. The band emission region of sample CA2.5C is apparently so broad that it almost spans from 650 to 1500 nm and could not be realized by any single RE ions. Furthermore, the emission region in 1200-1350 nm from Cr ions fills the spectral gaps of RE ions.

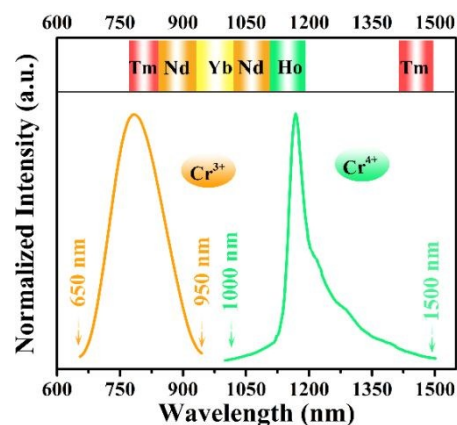


Figure 1 Observation of broadband emission of chromium activated aluminate glasses in 650-1500 nm: emission spectra of Cr doped aluminate glass (sample CA2.5C) upon excitation of 310 and 670 nm, respectively.

3.2. Strategies to enhance emission intensity and create new emission band in Cr activated aluminate glasses

Luminescence intensity has a strong dependence on the doping concentration of activator. Concentration optimization is a direct strategy to improve emission intensity and was firstly adopted in our work. Glasses doped with different Cr_2O_3 contents were prepared and illustrated in the inset of Figure 2(a). The glasses gradually turn to blue-green from originally colorless when doped Cr_2O_3 content increases. Absorption spectra can be exerted to analyze the characteristic electronic transitions of activators in materials. Herein the UV-NIR absorption spectra are in accordance with observed results. With introducing Cr_2O_3 , two strong absorption bands, i.e., at ~ 295 and 367 nm , from Cr^{6+} come into existence and obvious enhancement, which contributes to color changes directly. The intense absorption is associated with the charge transfer transition and manifests the oxidizing capacity of the aluminate glasses. Besides, a band, spanning the region of 500-1200 nm, is observed and originated from characteristic optical absorption of Cr^{4+} . The rich absorption region of Cr^{4+} ions could be roughly divided into three parts, that is, 520-840 nm, $\sim 1000\text{ nm}$, and $\sim 1150\text{ nm}$. The first absorption region is due to the transition of ${}^3\text{A}_2 \rightarrow {}^3\text{T}_1$ and the second could be attributed to the ${}^3\text{A}_2 \rightarrow {}^3\text{T}_2$

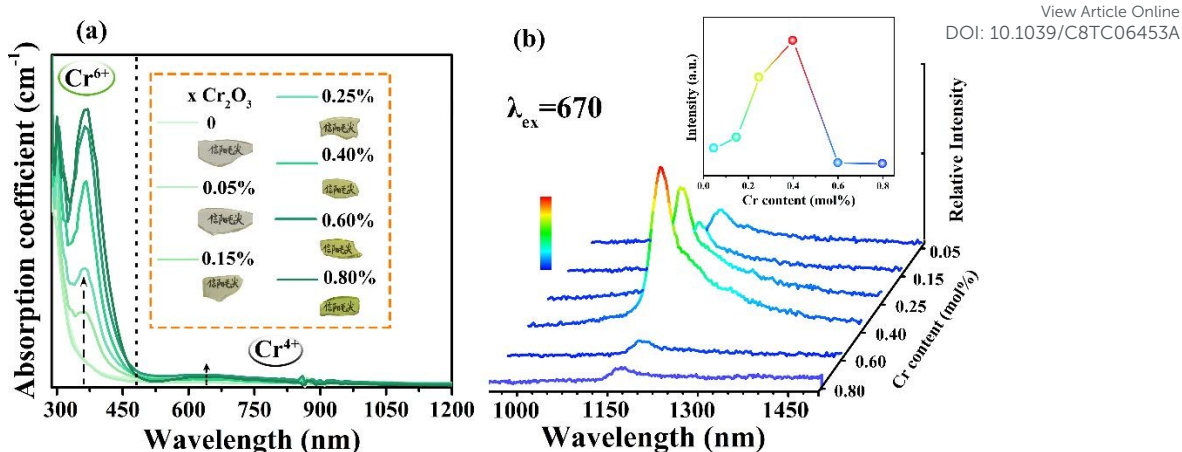


Figure 2. Concentration optimization of chromium dopant in Cr doped aluminate glasses. (a) absorption spectra and (b) emission spectra under 670 nm excitation of samples CAzC ($z=1000x$, $x=0, 0, 0.05\%, 0.15\%, 0.25\%, 0.40\%, 0.60\%, 0.80\%$); inset in Figure 2(b) shows the dependence of emission (~ 1175 nm) intensity on Cr content.

transition; the third absorption part results from the Fano antiresonance of the interaction between 1E and vibrationally broadened 3T_2 .^{25, 26, 34} In addition to these, the absorption band of Cr^{3+} was believed to be at around ~ 450 and 650 nm according to abundant researches, whose information might be obscured by Cr^{4+} ions absorption. Yet, the trace of Cr^{3+} in aluminate glasses could be confirmed by emission spectra (Figure 1).

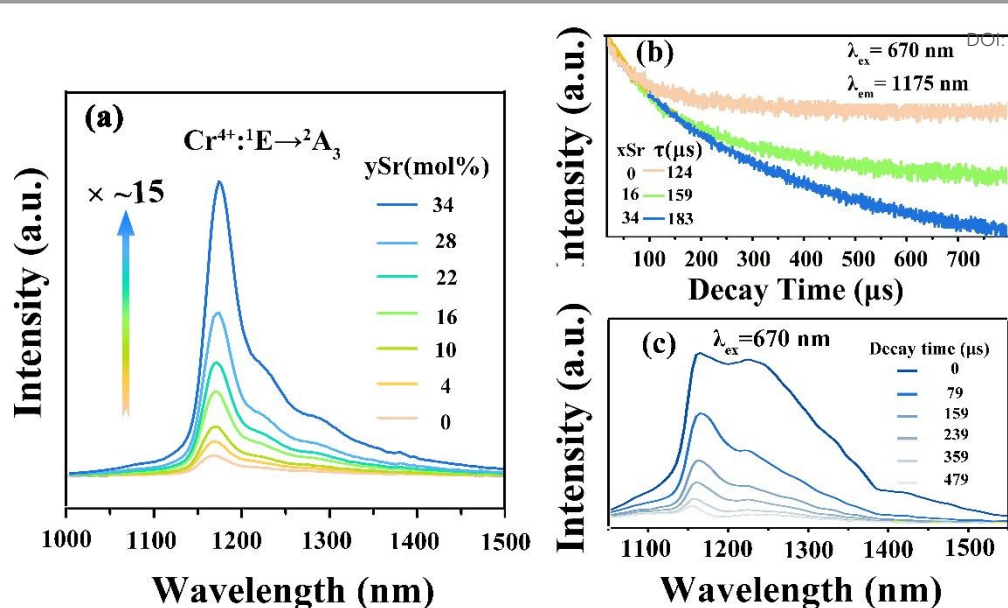
Figure 2(b) exhibits the emission spectra of aluminate glasses with different Cr contents. The line-like emission bands with the peak position at 1175 nm and a long tail extending down to 1500 nm were observed for all samples under 670 nm excitation. Such asymmetric emission covers the whole second telecommunication window. When increasing doping concentration of Cr, the emission intensity of Cr^{4+} goes rising initially and comes to a maximum at $x = 0.40$ mol%, as shown in the inset in Figure 2(b); subsequently, the emission intensity decreases, which might be induced by concentration quenching effect. The emission intensity is enhanced by about 5 times as compared to the sample of lowest content. Herein, 0.40 mol% Cr_2O_3 was the relatively optimal concentration for this system, yet for comparison, we selected 0.25 mol% Cr_2O_3 as experimental doping concentration in the following, since it is lower than critical content and the luminescence intensity is proportional to the content.

Aluminate glasses were verified to possess certain oxidizing capacity due to the encaged superoxide ion radical O_2^- , which leaves it possible to manipulate doped activators to be desired valence state.^{32, 33} And lack of traditional glass network former indicates relatively disordered structure and potentiates easier microstructure modulation, which provides a beneficial accommodation for activators.^{29, 35} Therefore, the optical properties of Cr doped aluminate glasses could be optimized by engineering aluminate glass structure and adjusting Cr ions valence state. After massive experiments, SrO was, thus, eventually considered as charming species in view of the fascinating evolutions of optical properties. In addition,

introducing certain SrO into aluminate glasses of notorious glass forming ability facilitates glasses preparation remarkably, which further pushes aluminate glasses one more step forward to the optical fiber. The quenched glasses samples tended to devitrificate and burst into fragments when removing SrO species. And differential scanning calorimetry (DSC) curves were adopted to quantitate the improved glass forming ability such as glass thermal stability. The formula $\Delta T = T_x - T_g$ is used to describe the glass thermal stability where T_x and T_g refer to the onset temperature of crystallization and glass transition temperature, respectively. The value of ΔT of certain SrO-contained aluminate glasses turns bigger than that of original aluminate glasses, for example, 70 , 140 and 119 K respectively corresponds to samples 0S, 10S and 22S, which indicates the improved glass forming ability under introducing certain SrO.

Figure 3(a) presents the emission spectra of chromium doped aluminate glasses under introducing different strontium oxides contents upon the excitation of 670 nm, characteristic emission from Cr^{4+} shows up in the range of 1050 – 1500 nm; meanwhile, it deserves mentioning that emission intensity keeps monotonically increasing along with SrO content. The intensity at the peak position of sample 34S is up to 15 times more than that of sample 0S. This is obviously more efficient to improve luminescence efficiency than concentration optimization (see inset in Figure 2(b)). Moreover, the tendency of enhancement by substitution has not exhibited an extremum point. However, it turns to be relatively hard to form amorphous glasses by virtue of limit cooling speed when the substituted CaO quantity by SrO exceeds 34 mol%. If glasses were successfully prepared via other feasible methods, such as sol-gel method and laser spin melting method, the enhancement might have not come to a stop.

The lifetime is the key factor to evaluate the spectroscopic performance. Luminescent decay curves of samples under the same testing conditions ($\lambda_{ex}=670$ nm, $\lambda_{em}=1175$ nm) were recorded respectively and listed as Figure 3(b). It is obvious that



View Article Online

DOI: 10.1039/C8TC06453A

Figure 3. Strategies to improve the optical performance of Cr⁴⁺ inside Cr activated aluminate glasses. (a) emission spectra of samples ySr (y=0, 4, 10, 16, 22, 28, 34) upon 670 nm excitation; (b) emission decay curves ($\lambda_{\text{ex}}=670$ nm, $\lambda_{\text{em}}=1175$ nm) of samples ySr (y=0, 16, 34); (c) time-resolved emission spectra of sample 34S ($\lambda_{\text{ex}}=670$ nm).

the decay time is prolonged along with the addition of SrO. The decay curves fit well the second order exponential equation $I(t) = A_1 \exp(-t/\tau_1) + A_2 \exp(-t/\tau_2)$, where $I(t)$ is the luminescent intensity at time t , A_1 and A_2 are constants, τ_1 and τ_2 are the lifetimes of fast and slow decays. The formula $\tau = (\tau_1 \tau_2^2 + A_2 \tau_1^2) / (A_1 \tau_1 + A_2 \tau_2)$ was used to calculate the mean lifetime of samples, and their average lifetimes are 124, 159 and 183 μs for samples 0S, 16S and 34S. The lifetime owns the same improvement tendency as that of ~ 1175 nm emission intensity when increasing SrO content. Meanwhile, the double exponential characters indicate the statistical distribution of multi-environments around Cr⁴⁺ potentially.

To justify the multi-centers of Cr⁴⁺ in aluminate glasses, time-resolved fluorescent spectra of sample 34S were performed under 670 nm excitation (Fig.3(c)). Apparently, the emission band consists of an abovementioned asymmetric line-like band and another broad band, originating from two luminescent centers of Cr⁴⁺ in different environments. The peak position of broadband emission locates at 1225 nm, which is attributed to the ${}^3T_2 \rightarrow {}^3A_2$ transition of Cr⁴⁺ in low-field sites, and the asymmetric band is due to the ${}^1E \rightarrow {}^3A_2$ transition of Cr⁴⁺ in high-field sites²⁷. As time goes, the line-shape is evolved from broad band into a relatively narrow one, because the emission at 1225 nm decays more quickly than that at ~ 1175 nm.

In addition to spectral evolutions of Cr⁴⁺ ions, the introduction of SrO results in great changes for the emission of Cr³⁺ ions. As shown in Figure 4(a), the red to deep-red emission spectra appear in typical Cr³⁺ emission region under 310 nm excitation. A broad band, centered at 785 nm, was observed for sample 0S, which comes from ${}^4T_2 \rightarrow {}^4A_2$ transition of Cr³⁺. Besides, when

substituting CaO with SrO, a new independent band, centered at ~ 708 nm, gradually develops and it becomes stronger than the original broad band eventually; and the two independent bands merge into an asymmetric band. The new band (~ 708 nm) could be ascribed to the transition of ${}^4T_2 \rightarrow {}^4A_2$ of Cr³⁺ in relatively higher crystal field³⁶. The evolution hints that two different sites of Cr³⁺ potentially coexist within higher SrO content samples. Other than this, the emission intensity of 785 nm goes down for ≤ 4 mol% SrO introduction (shown in Figure 4(b)); subsequently, it goes rising continuously and even overtakes that of sample 0S. These seem to be associated with the formation and ratio of new band at ~ 708 nm (discussed below in detail).

Likewise, time-resolved fluorescent spectra under 310 nm excitation were utilized to unravel the multi-luminescent centers of Cr³⁺ for sample 34S in the Figure 4(c). Initially, an asymmetric emission band, comprised of two bands centered at 708 and 785 nm respectively, is observed and the ~ 708 nm band dominates over the whole region. As delay is prolonged, the peak position of ~ 708 nm band is substituted by ~ 785 nm band. This is perhaps because ~ 708 nm band decays faster and transfers its energy to ~ 785 nm band. Therefore, at least two kinds of Cr³⁺ emission centers were created by introducing SrO.

From above results, two kinds of key evolutions happened to aluminate glasses when substituting CaO with SrO. On one hand, the emission intensity of Cr ions especially for Cr⁴⁺ comes to an obvious enhancement. On another hand, the new band, originating from Cr ions in new sites, is derived to further enrich emission region under introducing SrO. The reasons were explained below.

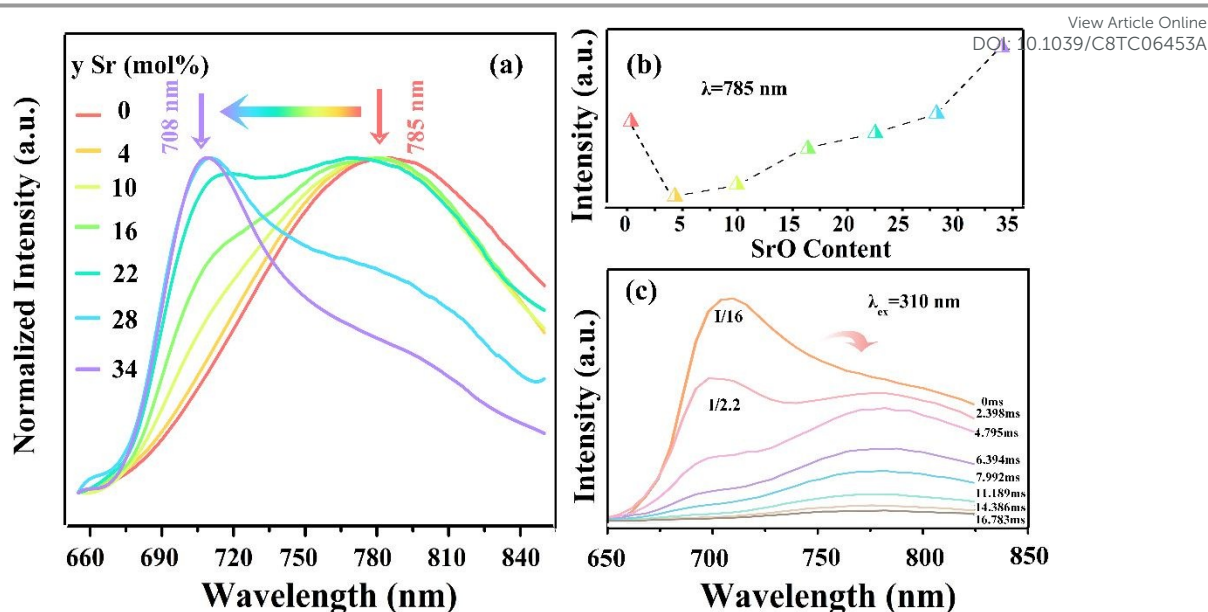


Figure 4. Creation of new emission center of Cr³⁺ with broadened and enhanced emission inside Cr doped aluminate glasses. (a) normalized emission spectra of samples yS (y=0, 4, 10, 16, 22, 28, 34) under 310 nm excitation; (b) dependence of 785 nm emission on SrO content; (c) time-resolved emission spectra of sample 34S ($\lambda_{\text{ex}}=310$ nm).

3.3 Mechanisms for enhanced luminescence intensity and new emission band in Cr activated aluminate glasses

Emission characters are closely associated with the absorption spectra, which together originate from distinct electronic transitions. Herein absorption spectra account for abovementioned evolution. Similarly, the featured absorption bands from Cr⁶⁺ (280-410 nm) and Cr⁴⁺ (500-1200 nm) ions can be resolved clearly, and absorption from Cr³⁺ ions could be picked out differently from its absorption region, overlapping with Cr⁴⁺ ions. To further discern variations on the ratio of Cr ions of different valence states qualitatively, absorption spectra were normalized to the absorption peak of Cr⁶⁺ (367 nm) and presented in Figure 5(b). Absorption intensity in the region (500-1200 nm) gradually keeps rising with SrO content, as shown in the inset of Figure 5(b). Though the region in 500-1200 nm might consist of Cr³⁺ and Cr⁴⁺ ions, we could speculate that introducing SrO facilitates the formation of more low-valence Cr ions (Cr³⁺ or Cr⁴⁺) from higher valence state.

The formation of Cr⁴⁺ was believed to be associated with O₂⁻, and it could be detected by EPR technology³⁷. Thence, EPR was adopted to dig out more information on Cr-related features and structure-related characters, especially for O₂⁻. As comparison, EPR spectrum of glass with no Cr doping is shown in Figure 5(c). The g value was calculated through the formula: $g = hv/\mu B$, where h is the Plank's constant, ν represents microwave frequency, μ refers to Bohr magneton and B is magnetic field strength. And the typical resonance at g=2.00 is observed, which is related to superoxide ion radical O₂⁻.^{32,33} With Cr doped

in glass, the resonance intensity of O₂⁻ goes down, and there exists a new resonance signal at g=1.96 due to Cr³⁺ ions³⁸. We infer that the decrease of O₂⁻ resonance intensity should be responsible for the formation of high-valence Cr ions. That is, Cr³⁺ doped could be oxidized to high-valence Cr ions by O₂⁻, which reduces the quantity of O₂⁻ and thus leads to decreasing resonance intensity. And these could be explained in the formulas: $3\text{Cr}^{3+} + \text{O}_2^- \rightleftharpoons 3\text{Cr}^{4+} + 2\text{O}^{2-}$, $3\text{Cr}^{4+} + 2\text{O}_2^- \rightleftharpoons 3\text{Cr}^{6+} + 4\text{O}^{2-}$ and $\text{Cr}^{3+} + \text{O}_2^- \rightleftharpoons \text{Cr}^{6+} + 2\text{O}^{2-}$.

EPR spectra under the same testing conditions for glasses of different SrO contents are presented in Figure 5(d). The intense resonance signals for all samples occur at g=2.00 (O₂⁻ related) and g=1.96 (Cr³⁺ related), and outlines of signal patterns almost stay unchanged. Yet, the intensity of O₂⁻ signal decreases with SrO content obviously and reaches its minimum under adding 16 mol% SrO; then the intensity starts to rise. On the other hand, Cr³⁺ ions related signal (g=1.96) keeps continuously decreasing, showing linear dependence on SrO content. This manifests the constant decrease of the content of trivalent Cr ions. Regarding the absorption overlap between Cr³⁺ and Cr⁴⁺ ions, the increased trend of absorption intensity in 500-1200 nm region, which would actually be undermined by less Cr³⁺ ions, is more able to reflect the increased content of Cr⁴⁺ ions. Hence by combining the analysis of absorption and EPR data, we could deduce that Cr⁴⁺ ions should be derived from Cr³⁺ or Cr⁶⁺ ions, which could be modulated by introducing SrO into aluminate glasses.

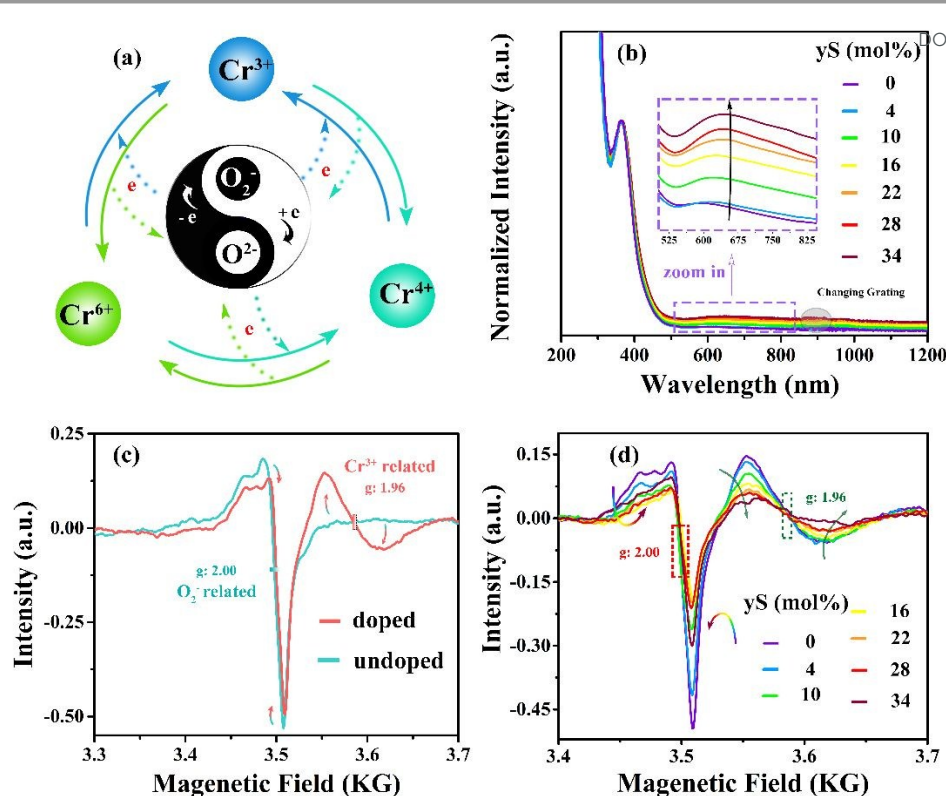


Figure 5. Mechanisms for the enhanced emission of Cr^{4+} in Cr activated aluminate glasses. (a) schematic for the redox of Cr ions within glasses with the existence of superoxide ion radical; (b) normalized absorption spectra of samples yS ($y=0, 4, 10, 16, 22, 28, 34$); (c) the EPR spectra of aluminate glasses with Cr doped and undoped (samples CA2.5C (or OS) and CAOC respectively); (d) EPR spectra of samples yS ($y=0, 4, 10, 16, 22, 28, 34$); inset in (b): zoom at the spectral region of 510 to 840 nm.

As analyzed above, the formation of high-valence Cr is associated with the superoxide ion radical O_2^- , and redox equilibrium among Cr^{3+} , Cr^{4+} and Cr^{6+} ions depends on the glass components closely, which determines the amounts of O_2^- directly. Therefore, with SrO content increased, there should be new redox equilibrium among Cr^{3+} , Cr^{4+} and Cr^{6+} ions. Considering the same Cr content for all glasses, continuous enhancement of Cr^{4+} absorption intensity under introducing SrO indicates that more Cr ions turn into tetravalence state through redox reaction. These are in accordance with the enhanced NIR emission intensity of Cr^{4+} . Hence, we speculate that oxidizing and reducing effects on Cr^{3+} and Cr^{6+} together lead to the variation of Cr^{4+} ratio and O_2^- amounts. Below 16 mol% SrO addition, the oxidizing effect on Cr^{3+} , rather than reducing effect on Cr^{6+} , dominates over the whole chain redox reaction, which consumes O_2^- amounts evidenced by EPR spectra. Yet, for samples containing more than 16 mol% SrO, reduction effect on Cr^{6+} ions mainly takes over the chain reaction, giving rise to superoxide ions radical contents. In addition, over the whole routine, the balance of chain reaction mainly leans to the middle section, which makes Cr^{4+} ions quantity keep increasing. The self-redox of Cr ions could be selective through SrO content, and Cr ions could be transformed into the desired valence state (the schematic is presented in Figure 5(a)).

The emission of Cr ions strongly depends on the crystal field surrounded. Thus, appearance of the new band (~ 708 nm), corresponding to new sites, should be related to matrixes structure. Structure-related information is obtained below to find more clues.

Emission located in the low-wavelength region (~ 708 nm), was originated from relative higher field sites of Cr, as compared to that at ~ 785 nm. X-ray powder diffraction could reflect the crystalline-related information and, thus, was performed on these samples with SrO introduced. As exhibited in the Fig6(a), obvious hump could be observed in the XRD patterns for all samples, and there are no diffraction peaks of crystal phase. These indicate that glasses maintained the intrinsic amorphous state without crystals precipitated. The shape and peak position of diffused hump are independent on the quantity variation of SrO. Yet, there occur remarkable changes in the intensity and width of humps. To describe this tendency, the integrated intensity of humps ($20\text{-}40^\circ$) were calculated in Figure 6(b). The integrated intensity stays unchanged firstly; and subsequently, beyond 10 mol% substitution, it almost linearly increases with SrO content. Meanwhile, we calculated the effective width ($\Delta\theta_{\text{eff}}$) to quantitatively describe the variations through the

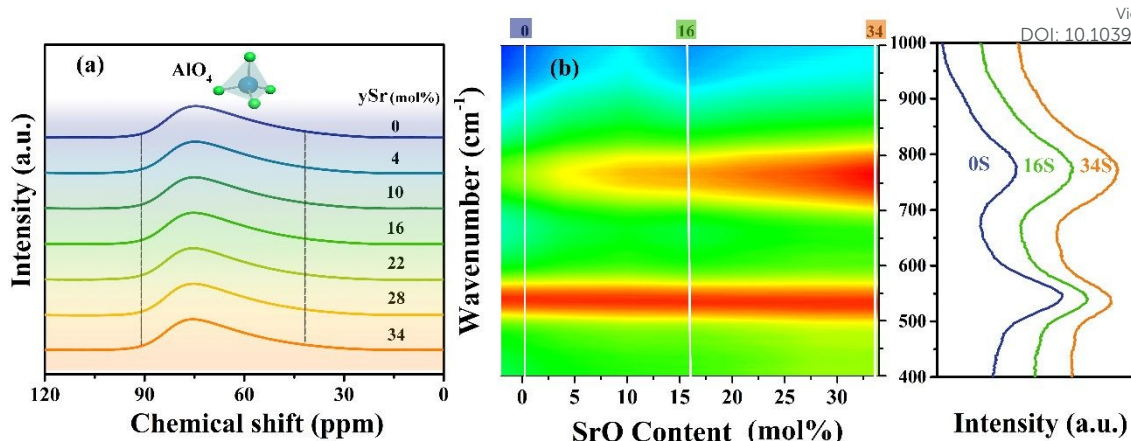


Figure 7. Structural evolutions of aluminate glasses with different SrO contents. (a) ^{27}Al MAS NMR spectra and (b) Raman spectra of samples yS ($y=0, 4, 10, 16, 22, 28, 34$).

From above analysis, substitution for CaO with SrO in glasses leads to glasses structure changes but maintains the main features especially for its amorphous characters. As revealed by ^{27}Al MAS NMR, Al is coordinated by four oxygens and serves as glass network formers, which is not influenced by SrO content significantly. In the meantime, the addition of SrO provokes depolymerization glass network and gives rise to more nonbridging oxygens. This enables glass to provide many potential micro-structures for Cr ions to reside, such as luminescent centers of tetrahedrally coordinated Cr^{4+} and octahedrally coordinated Cr^{3+} . Moreover, the depolymerization of glass network makes it relatively easy for glass to adjust its structure, which induces two kinds of sites for Cr ions on observation of XRD patterns (Figure 6) and spectroscopic data (Figure 4(a)).

4. Conclusion

In summary, broadband emission has been realized via doping Cr ions into aluminate glasses, where 650-950 nm and 1000-1500 nm emissions are derived from Cr^{3+} and Cr^{4+} ions. The broad emission region could hardly be realized merely by virtue of traditional RE ions. More importantly, selective self-redox and crystal field modulation have been demonstrated to improve the emission intensity and broaden emission region. The emission intensity is enhanced by one order due to massive Cr ions transformation into Cr^{4+} ions as emission centers through self-redox. Moreover, a new band at ~ 708 nm is created owing to the Cr^{3+} sites of relatively high crystal field and it enriches the emission region of the glasses. This method not only realizes enhanced and tuned broadband emission, potentially used for laser materials, but also sets an example for optical materials with polyvalent activators doped.

Conflicts of interest

There are no conflicts to declare.

Acknowledgements

We acknowledge financial supports from Guangdong Natural Science Foundation (Grant No. 2018B030308009), National Natural Science Foundation of China (Grant No. 51672085), Program for Innovative Research Team in University of Ministry of Education of China (Grant No. IRT_17R38), the Joint Fund of Ministry of Education of China (Grant No. 6141A02033225), Local Innovative Research Team Project of "Pearl River Talent Plan" (Grant No. 2017BT01X137) and Fundamental Research Funds for the Central Universities.

Notes and references

1. F. Bonaccorso, Z. Sun, T. Hasan and A. C. Ferrari, *Nature Photonics*, 2010, **4**, 611-622.
2. L. M. Tong, R. R. Gattass, J. B. Ashcom, S. L. He, J. Y. Lou, M. Y. Shen, I. Maxwell and E. Mazur, *Nature*, 2003, **426**, 816-819.
3. M. Peng, J. Qiu, D. Chen, X. Meng, I. Yang, X. Jiang and C. Zhu, *Opt. Lett.*, 2004, **29**, 1998-2000.
4. L. P. Wang, N. J. Long, L. H. Li, Y. Lu, M. Li, J. K. Cao, Y. Zhang, Q. Y. Zhang, S. H. Xu, Z. M. Yang, C. B. Mao and M. Y. Peng, *Light Sci. Appl.*, 2018, **7**, 1.
5. J. Cao, L. Li, L. Wang, X. Li, Z. Zhang, S. Xu and M. Peng, *J. Mater. Chem. C*, 2018, **6**, 5384-5390.
6. L. Tan, S. Kang, Z. Pan, Y. Zhang, Y. Yue, S. Xu, M. Peng and L. Wondraczek, *Adv. Opt. Mater.*, 2016, **4**, 1624-1634.
7. M. Peng, G. Dong, L. Wondraczek, L. Zhang, N. Zhang and J. Qiu, *J. Non-Cryst. Solids*, 2011, **357**, 2241-2245.
8. B. Wang, H. Lin, F. Huang, J. Xu, H. Chen, Z. Lin and Y. Wang, *Chem. Mater.*, 2016, **28**, 3515-3524.
9. S. Taccheo, G. Della Valle, R. Osellame, G. Cerullo, N. Chiodo, P. Laporta, O. Svelto, A. Killi, U. Morgner, M. Lederer and D. Kopf, *Opt. Lett.*, 2004, **29**, 2626-2628.
10. Q. Wang, J. Geng, T. Luo and S. Jiang, *Opt. Lett.*, 2009, **34**, 3616-3618.
11. G. Gao, M. Peng and L. Wondraczek, *J. Mater. Chem. C*, 2014, **2**, 8083-8088.
12. D. Chen, S. Liu, W. Xu and X. Li, *J. Mater. Chem. C*, 2017, **5**, 11769-11780.

13. M. Ding, D. Chen, D. Ma, J. Dai, Y. Li and Z. Ji, *J. Mater. Chem. C*, 2016, **4**, 2432-2437.
14. D. Chen, Y. Wang, Y. Yu, P. Huang and F. Weng, *J. Solid State Chem.*, 2009, **40**, 2763-2767.
15. H. Lin, D. Chen, Y. Yu, A. Yang and Y. Wang, *Opt. Lett.*, 2011, **36**, 1815-1817.
16. M. A. Hayward and M. J. Rosseinsky, *Nature*, 2007, **450**, 960-961.
17. E. Sharp, J. Miller and M. Weber, *Phys. Lett. A*, 1969, **30**, 142-143.
18. L. Tong, X. Li, J. Zhang, S. Xu, J. Sun, H. Zheng, Y. Zhang, X. Zhang, R. Hua, H. Xia and B. Chen, *Opt. Express*, 2017, **25**, 16047-16058.
19. X. Wang, X. Li, H. Zhong, S. Xu, L. Cheng, J. Sun, J. Zhang, L. Li and B. Chen, *Sci. Rep.*, 2018, **8**, 5736.
20. E. Sorokin, S. Naumov and I. T. Sorokina, *IEEE J. Sel. Top. Quant.*, 2005, **11**, 690-712.
21. I. T. Mckinnie and R. Y. Choie, *Opt. Quant. Electron.*, 1997, **29**, 605-610.
22. J. Xu, D. Chen, Y. Yu, W. Zhu, J. Zhou and Y. Wang, *Chem.-Asian J.*, 2015, **9**, 1020 – 1025.
23. B. Wang, H. Lin, Y. Yu, D. Chen, R. Zhang, J. Xu and Y. Wang, *J. Am. Ceram. Soc.*, 2014, **97**, 2539-2545.
24. H. Lin, G. Bai, T. Yu, M. K. Tsang, Q. Zhang and J. Hao, *Adv. Opt.Mater.*, 2017, **5**.
25. X. Wu, H. Yuan, W. Yen and B. Aitken, *J. Lumin.*, 1995, **66**, 285-289.
26. U. Ho, H. Eilers, W. Yen, J. Hayden and M. Aston, *J. Lumin.*, 1994, **60**, 119-122.
27. X. Wu, S. Huang, U. Hömmerich, W. Yen, B. Aitken and M. Newhouse, *Chem. Phys. Lett.*, 1995, **233**, 28-32.
28. D. Chen, Z. Wan and Y. Zhou, *Opt. Lett.*, 2015, **40**, 3607-3610.
29. D. R. Neuville, L. Cormier, V. Montouillout and D. Massiot, *J. Non-Cryst. Solids*, 2007, **353**, 180-184.
30. J. R. Allwardt, S. K. Lee and J. F. Stebbins, *Am. Mineral.*, 2003, **88**, 949-954.
31. C. Huang and E. C. Behrman, *J. Non-Cryst. Solids*, 1991, **128**, 310-321.
32. H. Hosono and A. Yoshihiro, *J. Am. Ceram. Soc.*, 1987, **70**, C-38–C-39.
33. H. Hosono, K. Yamazaki and Y. Abe, *J. Am. Ceram. Soc.*, 1985, **68**, C-304.
34. S. Kück, K. Petermann, U. Pohlmann and G. Huber, *Phys. Rev. B*, 1995, **51**, 17323-17331.
35. M. M. Sebdani, J. C. Mauro, L. R. Jensen and M. M. Smedskjaer, *J. Non-Cryst. Solids*, 2015, **427**, 160-165.
36. D. Chen, Z. Wan and Y. Zhou, *Opt. Lett.*, 2015, **40**, 3607-3610.
37. T. Murata, M. Torisaka, H. Takebe and K. Morinaga, *J. Non-Cryst. Solids*, 1997, **220**, 139-146.
38. V. Singh, R. V. S. N. Ravikumar, G. Sivaramaiah, J. L. Rao and S. H. Kim, *Mater. Res. Bull.*, 2015, **61**, 183-188.
39. G. H. Yue, P. X. Yan and J. Wang, *J. Cryst. Growth*, 2005, **274**, 464-468.
40. A. Patterson, *Phys. Rev.*, 1939, **56**, 978.
41. J. Cao, L. Wondraczek, Y. Wang, L. Wang, J. Li, S. Xu and M. Peng, *ACS Photonics*, 2018, **5**, 4393-4401.
42. F. Rasheed, K. P. O'Donnell, B. Henderson and D. B. Hollis, *J. Phys.: Condens. Matter*, 1991, **3**, 3825-3840.
43. C. R. Kesavulu, R. P. S. Chakradhar, R. S. Muralidhara, J. L. Rao and R. V. Anavekar, *J. Alloys Compd.*, 2010, **496**, 75-80.
44. M. Licheron, V. Montouillout, F. Millot and D. R. Neuville, *J. Non-Cryst. Solids*, 2011, **357**, 2796-2801.

View Article Online
DOI: 10.1039/C8TC06453A